Geophysical Research Letters

RESEARCH LETTER
10.1029/2024GL108849

Decrease in MJO Predictability Following Indo–Pacific Warm Pool Expansion

Hyemi Kim[1,2]

[1]Department of Science Education, Ewha Womans University, Seoul, Korea, [2]School of Marine and Atmospheric Sciences, Stony Brook University, Stony Brook, NY, USA

Abstract The characteristics of the Madden–Julian oscillation (MJO) have changed and are projected to continue changing with the expansion of the Indo–Pacific warm pool, which is the Earth's largest region of warm sea surface temperatures (SSTs). However, the likelihood of a change in MJO predictability following warm pool expansion remains unaddressed. Therefore, this study investigated the effect of warm pool expansion on MJO variability and predictability using the highly idealized aquaplanet configuration of Community Earth System Model 2 (CESM2). By expanding the warm pool in the Indo–Pacific, MJO-like waves become more regionally confined, short-lived convective events with weaker magnitude and less robust eastward propagating signals, possibly due to stronger zonal SST gradients and wider meridional widths of the warm pool. Perfect-model ensemble forecast experiments revealed that the MJO predictability decreased by approximately 5 days, the forecast error proliferated, and the signal rapidly reduced following warm pool expansion.

Plain Language Summary The Madden–Julian oscillation (MJO) is a prominent mode of tropical intra-seasonal variability in which its convective anomalies drive anomalous circulation within the tropics and remotely in the extratropics, thus providing a "forecast of opportunity" for global weather and climate events. Over the decades, MJO characteristics have changed and are projected to continue changing with the expansion of the Indo–Pacific warm pool—the largest pool with the warmest ocean temperature on Earth. If warm pool expansion changes the MJO characteristics, it is likely that its predictability has changed and will continue to do so in the future. In this study, the change in MJO predictability by expanding the Indo–Pacific warm pool was explored using CESM2 aquaplanet model experiments. The results show that, with warm pool expansion, MJO predictability decreased by approximately 5 days. This decrease is primarily attributed to the change of the MJO-like waves into more regionally confined, short-lived convective events with weaker magnitude and less robust eastward propagating signals, owing to the change in SST and circulations.

Key Points:

- A sensitivity experiment was performed using Community Earth System Model 2 aquaplanet with different prescribed sea surface temperatures
- Expanding the Indo–Pacific warm pool makes the Madden–Julian oscillation-like waves less organized
- The warm pool expansion quickens the forecast error increase and predictability decrease

Supporting Information:

Supporting Information may be found in the online version of this article.

Correspondence to:

H. Kim,
hyemi.kim@ewha.ac.kr

Citation:

Kim, H. (2024). Decrease in MJO predictability following Indo–Pacific warm pool expansion. *Geophysical Research Letters*, *51*, e2024GL108849. https://doi.org/10.1029/2024GL108849

Received 20 FEB 2024
Accepted 8 MAY 2024

Author Contribution:

Conceptualization: Hyemi Kim
Data curation: Hyemi Kim
Formal analysis: Hyemi Kim
Funding acquisition: Hyemi Kim
Investigation: Hyemi Kim
Methodology: Hyemi Kim
Resources: Hyemi Kim
Validation: Hyemi Kim
Writing – original draft: Hyemi Kim
Writing – review & editing: Hyemi Kim

© 2024. The Authors. Geophysical Research Letters published by Wiley Periodicals LLC on behalf of American Geophysical Union.
This is an open access article under the terms of the Creative Commons Attribution License, which permits use, distribution and reproduction in any medium, provided the original work is properly cited.

1. Introduction

Over the past decade, internationally coordinated experiments and efforts have made significant progress in sub-seasonal predictions (Marriotti et al., 2020). Sub-seasonal predictions aim to predict weather events and climate phenomena with a lead time of 3 to 4 weeks, which was formerly referred to as a "predictability desert" until predictability sources were identified. One of the primary sub-seasonal predictability sources from the tropics is the Madden–Julian oscillation (MJO; Madden & Julian, 1972). The MJO is a prominent mode of tropical intra-seasonal variability in which its convective anomalies drive anomalous circulation within the tropics and remotely in the extratropics, thus providing a "forecast of opportunity" for global weather and climate events. Due to the significance of MJO in global sub-seasonal predictions, researches have focused on its response to climate change.

MJO characteristics have changed and are projected to continue changing due to the altering climate system (Maloney et al., 2019). In recent decades, the MJO has strengthened, propagated faster, and exhibited changes in its residence time. Moreover, studies have shown that the La Niña-like mean-state change after the 1999 climate shift promoted more frequent non-propagating MJO events (Wang & Wang, 2023). Climate model simulations have revealed diverse projections of MJO in a warmer climate: a projected increase in amplitude and frequency (Bui & Maloney, 2018; Chang et al., 2015), faster eastward propagation and eastward extension (Bui & Maloney, 2020; Rushley et al., 2019), and shorter timescales (Bui & Maloney, 2018; Subramanian et al., 2014), although a substantial amount of uncertainty remains (Maloney et al., 2019).

19448007, 2024, 13, Downloaded from https://agupubs.onlinelibrary.wiley.com/doi/10.1029/2024GL108849 by Ewha Womans University Library, Wiley Online Library on [30/10/2024]. See the Terms and Conditions (https://onlinelibrary.wiley.com/terms-and-conditions) on Wiley Online Library for rules of use; OA articles are governed by the applicable Creative Commons License

Given the significant changes observed in MJO over time, it is likely that its predictability has changed and will continue to do so. For example, if the MJO timescale shortens with more localized features than a well-organized planetary-scale structure, MJO becomes less predictable (Kim et al., 2018). Although previous studies have examined changes in MJO characteristics, MJO predictability in a changing climate has only explored recently. Using observations and fully coupled model simulations, Du et al. (2024) discovered that MJO predictability has extended by approximately 6 days over the past century due to anthropogenic warming. They speculated that MJO tends to show more organized patterns, exhibiting greater consistency from event to event, and propagating eastwards more smoothly following global warming, thereby contributing to increased predictability. However, the underlying physical reasons for the changes in MJO predictability remain unaddressed. Although using observations and fully coupled models is crucial for understanding future MJO predictability, disentangling the relative contributions of different anthropogenic and natural forcings to the projected evolution and predictability of MJO poses challenges. Consequently, this study focuses solely on the effect of changes in basic state sea surface temperature (SST) patterns, which mimic the Indo–Pacific warm pool expansion following global warming.

The Indo–Pacific warm pool (hereafter referred to as the warm pool) is Earth's largest region of warm SSTs, which exceed 28°C, serving as a global heat engine. Due to deep convection and significant latent heat release, the warm pool plays an essential role in climate variability, including tropical intra-seasonal variability (De Deckker, 2016; Fasullo & Webster, 1999; Roxy et al., 2019). Although the warm pool has warmed and expanded significantly owing to greenhouse gas-induced warming (Hoyos & Webster, 2012; Weller et al., 2016), considerable uncertainty exists (Park et al., 2022). Roxy et al. (2019) showed that the warm pool size doubled between 1981 and 2018 compared to 1900–1980, significantly influencing MJO characteristics: the duration of the MJO shortens over the Indian Ocean, while it becomes more persistent and longer over the Maritime Continent and the Western Pacific. If variations in the warm pool alter an MJO characteristic, the MJO predictability will likely change as the warm pool expands in the future. However, the influence of warm pool variations on MJO predictability has not yet been identified.

In this study, the impact of warm pool expansion on MJO predictability was explored using a reduced complexity model following Kim and Benedict (2023; hereafter, KB23). Using aquaplanet configuration, KB23 examined the sensitivity of MJO predictability to prescribed asymmetric SSTs, which resembles the warm pool pattern. By adding a water-covered terrain mimicking the Maritime Continent landmasses to the warm pool-like SSTs, KB23 examined the Maritime Continent barrier effect on MJO characteristics and predictability. While MJO predictability is approximately 6 weeks when prescribed with warm pool SSTs, consistent with theoretical estimates (Kim et al., 2018), it decreases to 4 weeks when the MJO is disturbed by the Maritime Continent. This study builds upon the experimental setup of KB23. However, while KB23 focused on the Maritime Continent barrier effect, this study focused on the effect of warm pool expansion on MJO predictability. Section 2 describes the model settings and experimental design. The impacts of warm pool expansion on the basic state and MJO predictability are discussed in Section 3, while Section 4 provides the summary and discussion.

2. Data and Model Experiments

This study employed the aquaplanet configuration of the National Center for Atmospheric Research Community Atmosphere Model Version 6.0 (NCAR CAM6), which is the same numerical model as CAM6 but with reduced boundary condition complexity. The aquaplanet model serves as a framework for testing hypotheses beyond simpler models while distilling the salient features of complex models (Hoskins et al., 1999). Because the Earth is entirely covered by water without sea ice or topography, the effects of the land surface, land–sea contrast, and land–atmosphere feedback on the MJO are absent. This study adopted the exact configuration of the CESM2 aquaplanet model from KB23, featuring a horizontal resolution of 0.9° × 1.25°, 32 vertical levels, and a finite-volume dynamical core. Additionally, carbon dioxide concentration was set to 348 ppm and seasonality was neglected using perpetual equinox insolation (341 W m^{-2}) (Medeiros, 2020). The default CAM6 model configuration was optimized by increasing the cumulus entrainment rate to 10 times larger than the default CAM6 to enhance the simulations of the tropical variability modes (KB23).

To examine the impact of warm pool expansion on MJO, 10-year perpetual runs were performed forced by two different configurations of fixed SST: Control (CTRL) and warm pool expansion (WPE) experiments. Following Neale and Hoskins (2000), a zonally symmetric "QOBS" SST profile resembling the observed zonal mean SST structure of March was defined as follows:

19448007, 2024, 13, Downloaded from https://agupubs.onlinelibrary.wiley.com/doi/10.1029/2024GL108849 by Ewha Womans University Library, Wiley Online Library on [30/10/2024]. See the Terms and Conditions (https://onlinelibrary.wiley.com/terms-and-conditions) on Wiley Online Library for rules of use; OA articles are governed by the applicable Creative Commons License

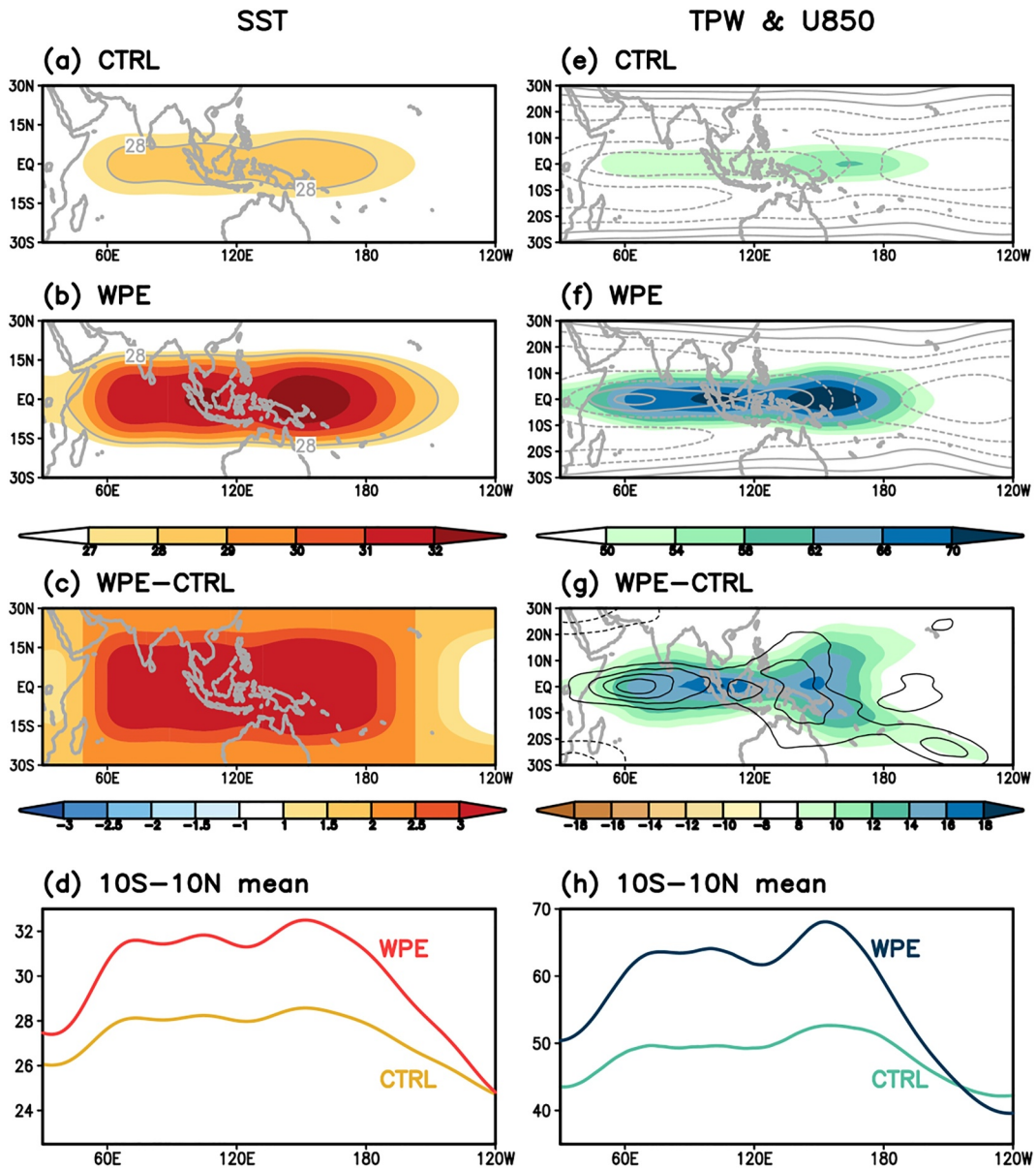


Figure 1. Climatology of sea surface temperature (SST) (°C) in the (a) CTRL, (b) warm pool expansion (WPE) runs, (c) WPE minus CTRL, and (d) average over 10°S–10°N. Climatological 28 °C isotherm is marked as gray contour in (a), (b). The right panel shows the total precipitable water (TPW) (shading, kg m^{-2}) and U850 (contour). (e)–(f) Solid and dash contours represent positive and negative U850, respectively (contour interval of 3 m s^{-1}), (g) their difference (contour interval of 1 m s^{-1}) and (h) TPW average over 10°S–10°N.

$$\mathrm{SST}_{\mathrm{QOBS}} = \frac{1}{2}\left[300\left(1-\sin^2\left(\frac{\pi\theta}{120}\right)\right)\right] + \frac{1}{2}\left[300\left(1-\sin^4\left(\frac{\pi\theta}{120}\right)\right)\right]$$

where θ (latitude in degrees) ranges between 60°S and 60°N. The QOBS SST profile has a global average of 14.85°C. March SST climatology (HadISST; Rayner et al., 2003) was used as an observed reference. The maximum SST of 26.85°C on the equator decreased to 0 °C at 60° latitude and remained uniformly at 0°C from 60° to the polar caps (Figure 1 in KB23). As a CTRL simulation, a fixed SST replicating the Indo–Pacific warm pool was applied (Figure 1a), with details of the SST pattern shaping and construction described in KB23. These warm pool-like SST experiments reasonably simulated the basic state, MJO, and tropical variability modes (Andersen & Kuang, 2012; Das et al., 2019; Kim & Benedict, 2023; Maloney & Wolding, 2015; Wu et al., 2021).

19448007, 2024, 13, Downloaded from https://agupubs.onlinelibrary.wiley.com/doi/10.1029/2024GL108849 by Ewha Womans University Library, Wiley Online Library on [30/10/2024]. See the Terms and Conditions (https://onlinelibrary.wiley.com/terms-and-conditions) on Wiley Online Library for rules of use; OA articles are governed by the applicable Creative Commons License

Notably, the CTRL simulation in this study is the same as the "WarmPool" run in KB23; thus, some of the CTRL run results presented here have been discussed in KB23. Therefore, we will briefly summarize the results from CTRL and focus on the WPE experiments.

The WPE experiment investigated the effect of warm pool expansion on MJO characteristics and predictability. The WPE SST was constructed as follows: First, 2°C was uniformly added to every grid point to the observed March SST, denoted as SST(x,y). Then, the SST departures (SST′(x,y)) were calculated from the zonal mean, and a meridional average of SST′(x,y) between 5°S and 5°N that results in a zonal profile SST′(x) were further smoothed by retaining 10 harmonics in longitude ($\widetilde{\text{SST}'}(x)$). Subsequently, the smoothed zonal profile of $\widetilde{\text{SST}'}(x)$ was applied from 30°S to 30°N, tapered to a weight of zero poleward of 30° South and North, and with a weight of 1.0 along the equator. Note that, except for adding 2°C to the observed March SST climatology, this approach is the same as that used in KB23. Figures 1a–1c depicts the prescribed SST pattern of the WPE run and its deviation from that of the CTRL run. SSTs in the WPE run can be as much as 3°C warmer in the Indo–Pacific than in the CTRL run (Figures 1a–1d). Although a 3°C increase in SSTs is somewhat unrealistic, this study examined the changes in MJO characteristics and predictability in an idealized framework. Because the SST was constructed to keep the globally averaged SST and the zonal mean SST profile the same as the observed structure, the increase in SST over the warm pool caused a sharp decrease in SST east of the dateline (180°E) (Figure 1c). Each perpetual run and forecast experiment prescribed with CTRL and WPE SSTs was simulated for 120 months (10 years), with the basic state, MJO variability and predictability compared in Section 3. Strictly speaking, warm pool expansion encompasses both increased SST and an expanded area of warm SST, rather than just the expansion itself. The warm pool area was estimated as the area covered by a climatological 28 °C SST isotherm (Figures 1a and 1b) within 40°E to 160°W, 20°S to 20°N. The area measured approximately 2×10^7 km^2 in the CTRL run and expanded to approximately 6×10^7 km^2 in the WPE run. This estimate of warm-pool area change aligns with Roxy et al. (2019), where the area ranged from 2×10^7 to 3×10^7 km^2 in the early 1900s and expanded to $\sim 6 \times 10^7$ km^2 after 2000.

3. Results

3.1. Warm Pool Expansion Effects on the Basic State and MJO-Like Waves

Changes in the basic state thermodynamic and dynamic fields were influenced by SST variations. The spatial distribution of the 10-year averaged climatology of total (vertically integrated) precipitable water (TPW) and zonal wind at 850 hPa (U850) followed the SST patterns (Figures 1e–1h). The total precipitation and Outgoing Longwave Radiation (OLR) climatology patterns resembled the TPW pattern (not shown), indicating increased convective activity where SSTs were warmer in both the CTRL and WPE runs (Figures 1e–1h). With warm pool expansion (WPE run), the amount of precipitable water over the warm pool was nearly 1.5 times larger than that in the CTRL run (Figures 1f and 1h), indicating that warmer SSTs foster greater convective activity. The circulation fields also changed as the SST increased. In the CTRL run, low-level easterly trade wind was simulated over the entire tropics (Figure 1e). However, in the WPE run, when a larger SST zonal gradient was prescribed, a low-level westerly appeared over the equatorial Indo–Pacific warm pool (Figures 1f–1h), indicating an enhanced Walker circulation. Previous studies have argued that background SST and related circulation fields can strongly modulate tropical intra-seasonal variability (Kang et al., 2013; Klingaman & Demott, 2020; Suematsu & Miura, 2018, 2022; Suematsu et al., 2022; Wang & Rui, 1990); this will be further discussed later.

To examine the changes in intra-seasonal variability following warm pool expansion, the tropically averaged (10°S–10°N) 20–100-day bandpass-filtered U850 anomalies over 500 randomly selected consecutive days are presented (Figures 2a and 2b), along with the intra-seasonal amplitude defined as a standard deviation of 20–100-day bandpass-filtered U850 anomalies over 10 years (Figures 2c and 2d). In both runs, convection was active over the warm pool area and significantly weakened when the SST decreased sharply. In the WPE run, eastward-moving intra-seasonal events became weaker and less frequent than in the CTRL run (Figure 2b). Furthermore, in both runs, the intra-seasonal wind activity appeared more or less spontaneously in a limited region, mainly over the warm pool (Figures 2c and 2d). Although the intra-seasonal amplitude was comparable in both runs, there was a slightly stronger magnitude in the WPE run over the western and eastern boundaries of the warm pool. Similar results were obtained when computing the intra-seasonal amplitude of other variables, such as OLR or precipitation (not shown). However, comparable intra-seasonal amplitudes between CTRL and WPE runs do

19448007, 2024, 13, Downloaded from https://agupubs.onlinelibrary.wiley.com/doi/10.1029/2024GL108849 by Ewha Womans University Library, Wiley Online Library on [30/10/2024]. See the Terms and Conditions (https://onlinelibrary.wiley.com/terms-and-conditions) on Wiley Online Library for rules of use; OA articles are governed by the applicable Creative Commons License

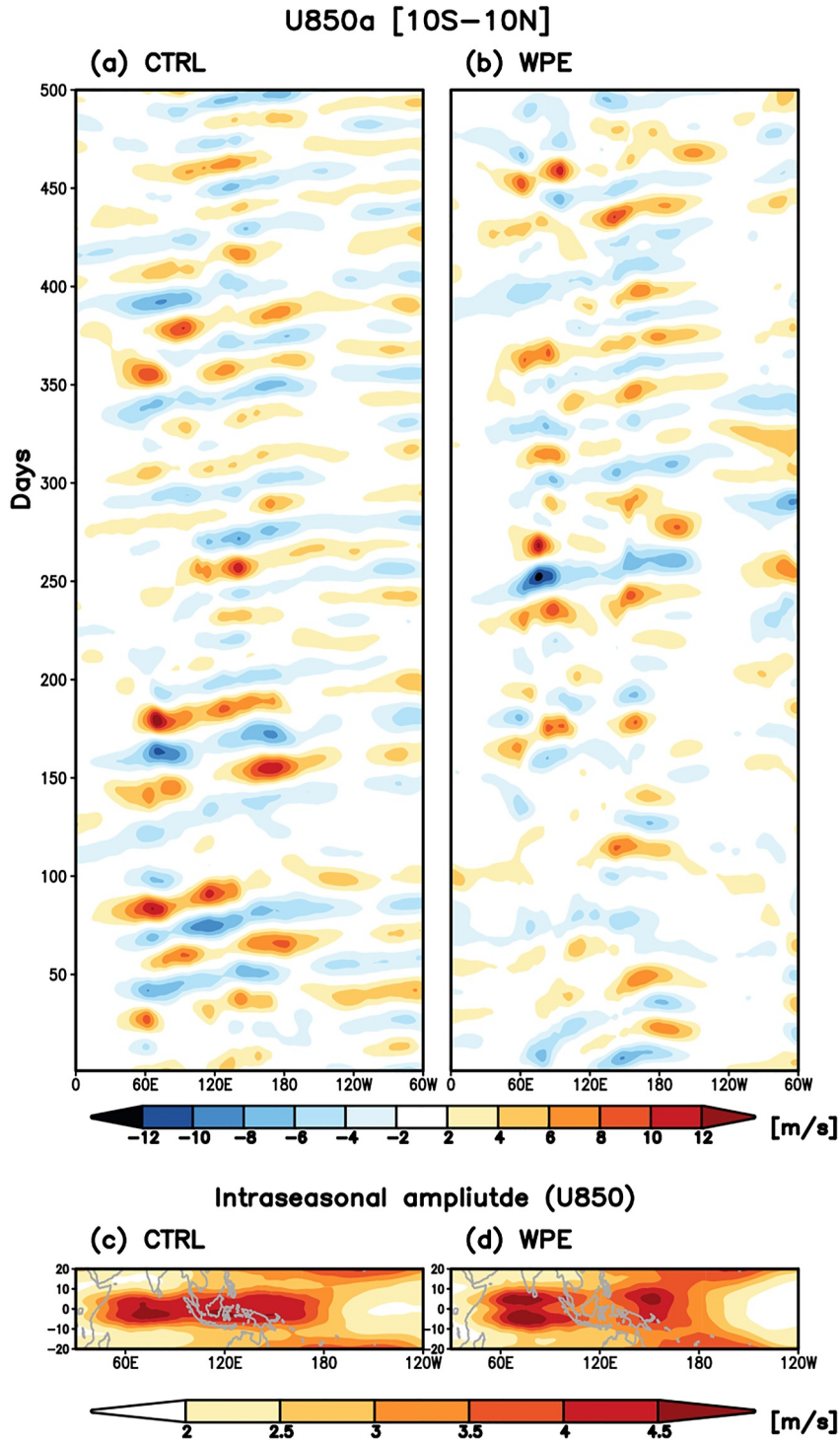


Figure 2. Daily U850 (m s^{-1}) anomaly averaged over 10°S–10°N during 500 randomly selected consecutive days in (a) CTRL and (b) WPE runs. Intra-seasonal amplitude (standard deviation of 20–100-day filtered U850 anomaly calculated over 120 months) in (c) CTRL and (d) WPE runs.

not directly indicate a comparable amplitude of MJO, as the intra-seasonal component is a mixture of many waves within the 20–100-day period.

To examine the MJO-like waves and convectively coupled equatorial waves (CCEWs), wavenumber–frequency spectral analysis was performed using daily OLR data averaged over the equatorial band (15°S–15°N). Figure S1

19448007, 2024, 13, Downloaded from https://agupubs.onlinelibrary.wiley.com/doi/10.1029/2024GL108849 by Ewha Womans University Library, Wiley Online Library on [30/10/2024]. See the Terms and Conditions (https://onlinelibrary.wiley.com/terms-and-conditions) on Wiley Online Library for rules of use; OA articles are governed by the applicable Creative Commons License

in Supporting Information S1 shows the ratio of the wave power to the total power in the symmetric components across the equator after removing the smooth empirical background noise spectrum (Wheeler & Kiladis, 1999). In the CTRL run (Figure S1a in Supporting Information S1), the overall shape of the power spectrum for the CCEWs was close to the observed; however, the simulated Kelvin wave and equatorial Rossby wave exhibited slower speeds and weaker signals than the observed (observation shown in KB23; Figure 5a). The maximum power of the MJO-like wave in the CTRL run exceeded that of the observed. However, the power shifted to a higher frequency (faster speed) than in the observed, with a period of approximately 25 days, concentrated broadly at wave numbers 1–3. Although the frequency does not exactly match the observation, it is acceptable, given the highly simplistic design of the aquaplanet. The east/west ratio (E/W ratio) is a measure of the MJO eastward-propagating feature, which is obtained by dividing the sum of the spectral power over the "MJO band" (30–60 days, wave numbers 1–3) by that of its westward-propagating counterpart (Ahn et al., 2017). CTRL showed a weaker E/W ratio (1.8) than the observed (2.4), consistent with most CMIP models (Ahn et al., 2017). In the WPE run (Figure S1b in Supporting Information S1), both the eastward and westward powers weakened compared to CTRL, and the maximum of the MJO-like wave shifted to wave number one but in a higher frequency band, indicating a shorter period (~20 days). Due to the higher power reduction in the eastward band, the E/W ratio decreased to 1.4 in the WPE run.

To examine the MJO-like variability and its patterns, real-time multivariate MJO indices (RMM; Wheeler & Hendon, 2004) were calculated from the 10-year perpetual runs with the OLR and zonal wind at 850 and 200 hPa, respectively. The leading eigenvectors (Figure S2 in Supporting Information S1) of the combined empirical orthogonal function (CEOF) from the model simulations were close to the observed despite the simplified model configuration. Based on the MJO phase defined by the simulated RMM indices, the 2D pattern of the MJO-like mode was compared in the composite analysis of the 20–100 filtered 850 hPa horizontal wind and OLR anomalies (Figure S3 in Supporting Information S1). The corresponding observational results are available in Figure 1 by Kim et al. (2018). Similar to the aforementioned results, strong MJO activity over the warm pool and a robust eastward propagation signal with decay over the Eastern Pacific were well captured in the CTRL run (Figure S3a in Supporting Information S1). Conversely, with warm pool expansion, the MJO-like wave signal became weaker and less organized than in the CTRL run (Figure S3b in Supporting Information S1), consistent with the wavenumber–frequency analysis results.

Lag regression analysis was performed to further investigate the effect of warm pool expansion on the eastward propagation of MJO-like waves. Figure 3 shows the regression coefficients of the 20–100-day bandpass-filtered OLR and U850 anomalies against the reference points, which are the intra-seasonally filtered OLR time series over the Eastern Indian Ocean (60°–90°E and 10°S–10°N). Subsequently, the regression coefficients were averaged over 10°S–10°N. In the CTRL run (Figure 3a), the eastward-propagating MJO signals were well captured, exhibiting a near-quadrature phase relationship between low-level circulation and convective anomalies. This baroclinic wave structure helps the MJO propagate eastward by supplying anomalous moisture to the east of the convection (Adames & Kim, 2016; Jiang et al., 2020). Conversely, with warm pool expansion, although some weak low-level wind signals showed propagation, the MJO eastward-propagating convective signal was absent, and the convection was confined to the region where it was initiated (Figure 3b).

In summary, with warm pool expansion, MJO-like waves became more regionally confined, short-lived convective events with weaker magnitude and less robust eastward-propagating signals. These changes may be attributed to basic-state SST, moisture patterns, and associated circulation changes (Figure 1). The SST structure determines the horizontal structure of the coupled Kelvin–Rossby waves, whereas the relative amplitude of these waves further determines the MJO amplitude and phase speed (Wang & Rui, 1990). Prior studies have shown that MJO characteristics are strongly influenced by the background SST distribution in observations (Suematsu & Miura, 2018, 2022) and simulations (Kang et al., 2013; Klingaman & Demott, 2020; Suematsu et al., 2022). The zonal SST gradient was stronger in the WPE run than in CTRL, and the meridional width of the warm SST region expanded further (Figure 1). These two effects significantly influenced the behavior of MJO-like waves. When the SST was prescribed with a stronger zonal gradient, a low-level westerly appeared over the equatorial Indo–Pacific warm pool, indicating an enhanced Walker circulation (Figures 1f–1h). Previous studies have shown that MJO tends to decelerate, and convection becomes more regionally confined, short-lived events when the thermally direct Walker circulation is intensified by the large zonal SST gradients (Suematsu & Miura, 2018, 2022). This aligns with previous findings, whereby the observed MJO convective activities tended to be confined westward of the dateline during the La Niña phase (stronger Walker circulation). In contrast, MJO

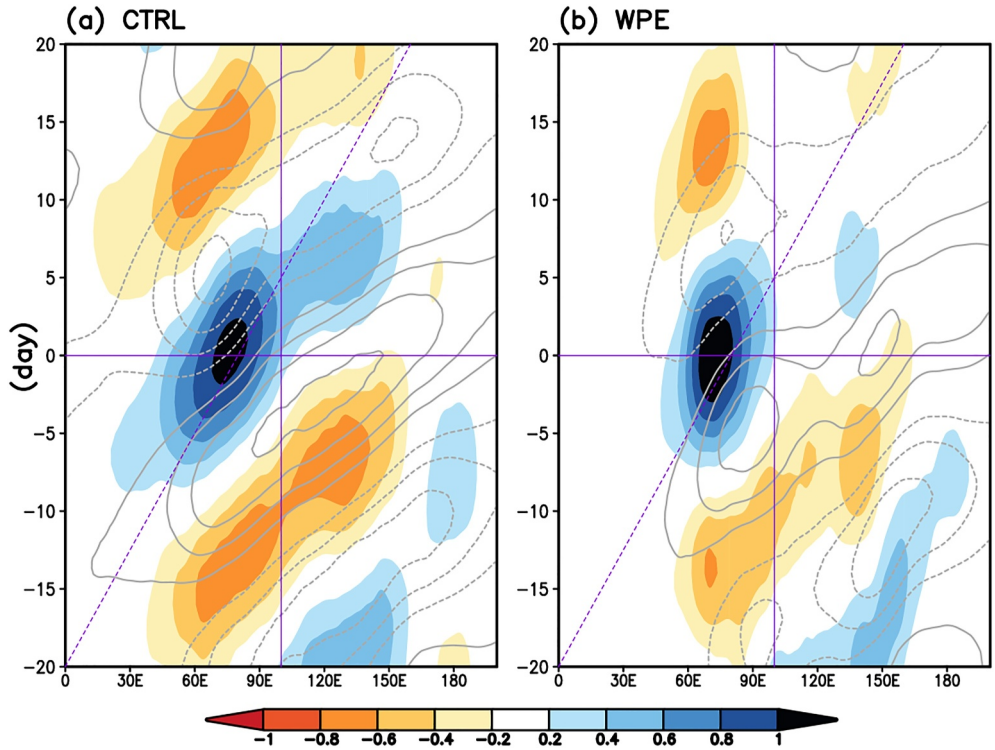


Figure 3. Lag regression coefficients of anomalous Outgoing Longwave Radiation (OLR) (W m^{-2}) and U850 (m s^{-1}) in (a) CTRL and (b) WPE runs. The regression coefficient of 20–100-day band-pass-filtered anomalies against OLR averaged over the equatorial Eastern Indian Ocean (60°E–90°E, 10°S–10°N) is displayed. Coefficients are averaged over 10°S–10°N. Positive regression coefficients (blue shading and solid contours) indicate negative OLR and easterly U850. Purple dashed lines denote the 5 m s^{-1} phase speed, which is close to the observed MJO phase speed, while purple solid lines indicate 0-lag (*x*-axis) and 100°E (*y*-axis).

activities extend beyond the dateline during the El Niño phase (Hendon et al., 2007; Pohl & Matthews, 2007; Woolnough et al., 2000). A recent study by Wang and Wang (2023) revealed that the frequency of the standing oscillation events of the MJO, which corresponds to the non-propagating MJO events, increased due to the La Niña–like mean-state change associated with the 1999 climate shift. In addition, the wind-induced surface heat exchange theory argues that, in the presence of mean tropical low-level easterlies, enhanced surface fluxes to the east of MJO convection supports the eastward propagation (Fuchs & Raymond, 2017; Shi et al., 2018). Conversely, the mean westerlies enhanced in the WPE run (Figures 1f and 1g) may have contributed to weaker MJO propagation (Sobel & Maloney, 2013). The meridional broadening of the warm SST area can also impact the equatorial wave activities (Jiang et al., 2020). Using aquaplanet simulation, Kang et al. (2013) demonstrated that when the meridional width of the high SST region broadens, the fast, unstable Kelvin waves slow down and weaken, while westward-propagating Rossby waves excite more due to off-equatorial moisture supply, consequently weakening the eastward propagating wave. Further sensitivity experiments with zonal and meridional narrowing and widening of the warm pool could help confirm these hypotheses.

3.2. Warm Pool Expansion Effects on MJO Predictability

The primary purpose of this study is to understand how MJO predictability changes as the warm pool expands. Based on KB23, it was concluded that when the MJO is weaker and regionally confined due to the Maritime Continent propagation barrier, its predictability decreases by approximately 10 days. In the WPE run, the MJO-like wave weakened and became confined to regionally short-lived convective events, indicating a likely decrease in MJO predictability. To test this hypothesis, we performed perfect-model ensemble forecast experiments with and without WPE, similar to KB23 (Figure S4 in Supporting Information S1). We briefly explain the step here, with the details described in KB23. First, 10-year perpetual runs using CTRL and WPE SSTs were performed, considering these perpetual runs as the "truth." In these perpetual runs, restart files were saved every 10 days.

19448007, 2024, 13, Downloaded from https://agupubs.onlinelibrary.wiley.com/doi/10.1029/2024GL108849 by Ewha Womans University Library, Wiley Online Library on [30/10/2024]. See the Terms and Conditions (https://onlinelibrary.wiley.com/terms-and-conditions) on Wiley Online Library for rules of use; OA articles are governed by the applicable Creative Commons License

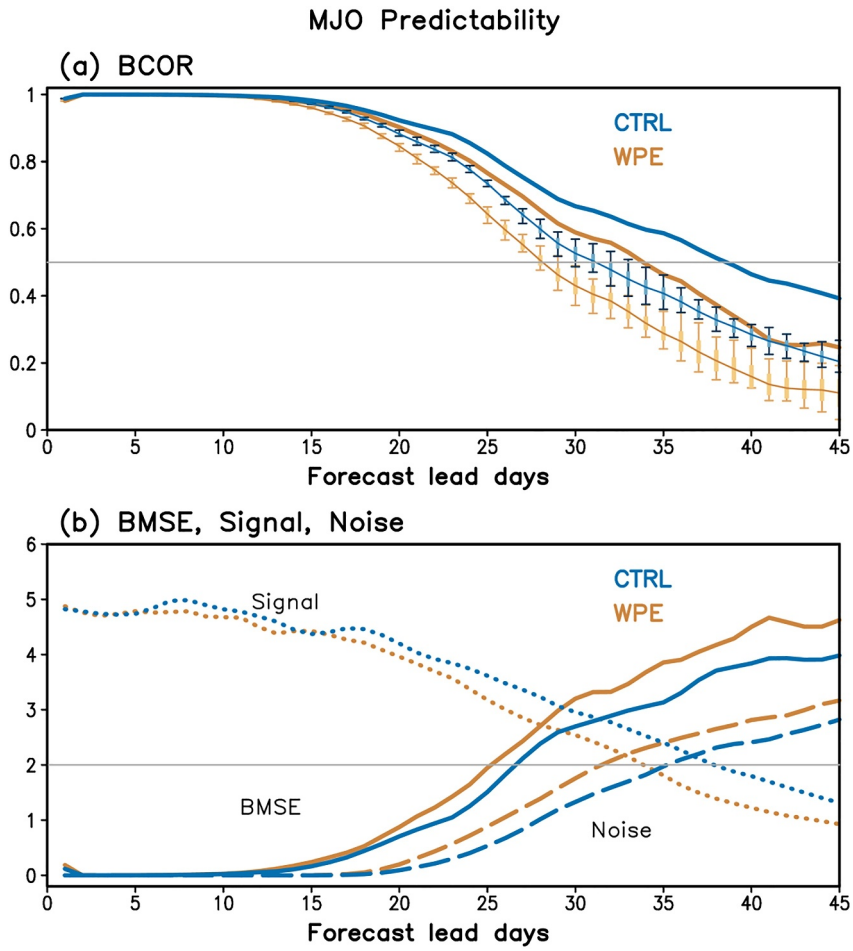


Figure 4. MJO predictability assessed by (a) BCOR, (b) BMSE (solid), signal (dot lines), and noise (dashed lines) for CTRL (blue) and WPE (brown) runs. The thick lines represent the skill in the ensemble mean, and the thin lines indicate the average of the skill from individual ensembles. The box–whisker plots represent the spread of skill. The box outlines the ±1.0 standard deviation of skill, and whiskers indicate the minimum and maximum values. Gray horizontal lines in (a) and (b) indicate the arbitrarily chosen values of 0.5 and 2.0, respectively.

From each restart file, the model was integrated for 45 days, each consisting of 10 ensemble members, resulting in 360 cases of 45-day forecast sets (10-year × 36 cases/year). Subsequently, the 45-day forecasts in each CTRL and WPE run were compared with their corresponding truth. A comparison of the predictability between the CTRL and WPE runs indicated a change in predictability caused by the warm pool expansion. To obtain the forecasted RMM indices, the forecasted anomalies from the CTRL and WPE runs were projected onto the eigenvectors of the observed CEOF (Figure S2 in Supporting Information S1) and normalized. Then, bivariate correlation coefficient (BCOR), bivariate root mean squared error (BMSE), signal, and noise were calculated in the same manner as KB23 (please see the details for the calculation). Due to the limited sample size, the results for all MJO phases are presented rather than dividing them into eight phases.

For the CTRL run, the BCOR of the ensemble mean showed an approximately 5.5-week (day 39) skill when using BCOR = 0.5 as a reference (Figure 4a), consistent with the theoretical MJO predictability estimate (Kim et al., 2018). However, with warm pool expansion, the BCOR skill decreased to approximately 5 weeks (day 34) because of the less organized and short-lived events, a decrease of approximately 5 days compared to the CTRL run. When the BCOR of the single ensembles was calculated and averaged, it decreased by approximately 1 week compared to the ensemble means in both the CTRL and WPE forecasts (Figure 4a). The BMSE increased and reached the 2.0 line (arbitrarily chosen threshold) on day 24 in the WPE simulation, approximately 2–3 days earlier than in CTRL (Figure 4b). In the CTRL run, the MJO forecast signal (variability of ensemble–mean) gradually decreased, reaching the 2.0 line (arbitrarily chosen threshold) at day 37. The signal decreased faster in

19448007, 2024, 13, Downloaded from https://agupubs.onlinelibrary.wiley.com/doi/10.1029/2024GL108849 by Ewha Womans University Library, Wiley Online Library on [30/10/2024]. See the Terms and Conditions (https://onlinelibrary.wiley.com/terms-and-conditions) on Wiley Online Library for rules of use; OA articles are governed by the applicable Creative Commons License

19448007, 2024, 13, Downloaded from https://agupubs.onlinelibrary.wiley.com/doi/10.1029/2024GL108849 by Ewha Womans University Library, Wiley Online Library on [30/10/2024]. See the Terms and Conditions (https://onlinelibrary.wiley.com/terms-and-conditions) on Wiley Online Library for rules of use; OA articles are governed by the applicable Creative Commons License

the WPE run and reached the threshold on day 34 (Figure 4b). Additionally, the forecast noise (ensemble spread) was larger in the WPE run than in CTRL. The BMSE consistently exceeded the noise in both configurations, indicating that both ensemble forecast systems are under-dispersive and, consequently, unreliable. In summary, the predictability of the MJO-like waves decreases because of the increase in the less-organized locally confined events following warm pool expansion.

4. Summary and Discussion

This study examined the changes in MJO variability and predictability by expanding the warm pool using CESM2 aquaplanet experiments, where different patterns of SSTs were prescribed. By expanding the Indo–Pacific warm pool, MJO-like waves became more short-lived and regionally confined convective events with weaker magnitudes and less robust eastward-propagating signals. The stronger zonal SST gradient, enhanced Walker circulation, and wider meridional width of the warm SST region in the WPE run may have contributed to the less organized behavior of the MJO-like waves, consistent with previous studies. However, sensitivity experiments with zonal and meridional variations in warm-pool SST distributions should be performed to confirm these hypotheses. MJO predictability was estimated by performing perfect-model ensemble experiments. Based on the correlation coefficient, the MJO predictability decreased by approximately 5 days, the forecast error increased faster, and the signal reduced faster when the warm pool was expanded. The implication of this study to the scientific community is that if the warm pool continues to increase, the MJO is likely to become less organized, regionally confined, and have a shorter period, contributing to its predictability loss. The Maritime Continent barrier effect was not considered in both CTRL and WPE runs. However, from KB23, it is reasonable to estimate that adding the Maritime Continent to the WPE run would further decrease MJO predictability, resulting in approximately 3 weeks of predictability, three weeks lower than the theoretical estimate (KB23). The implication relevant to the numerical modeling community is that realistic simulation of the basic states and their long-term variation (e.g., ENSO) is crucial for better MJO simulation and prediction. Notably, this study does not contradict Du et al. (2024), who suggested that MJO predictability has increased and is likely to grow in warmer climates using observational data and future projections from climate models. This study focused solely on the effect of the basic-state SST patterns on MJO predictability in a highly idealized model world. Similar experiments with a more realistic configuration of the Earth's system using multi-models could help address the uncertainty level attached to MJO predictability in future climates.

Data Availability Statement

The HadISST data sets were obtained from the Met Office Hadley Centre (https://www.metoffice.gov.uk/hadobs/hadisst/). Output from CESM2 simulations and codes used for analysis are available at Kim (2024).

Acknowledgments
Constructive and valuable comments from two anonymous reviewers are greatly appreciated. H. Kim was supported by the National Research Foundation of Korea (NRF) Grant funded by the Korean government (NRF-RS-2023-00278113) and NOAA Grant NA22OAR4590168. This material is based upon work supported by the National Center for Atmospheric Research (NCAR), a major facility sponsored by the NSF under Cooperative Agreement No. 1852977. The CESM project is supported primarily by the NSF. We would like to acknowledge high-performance computing and data storage support from Cheyenne (https://doi.org/10.5065/D6RX99HX) provided by NCAR's Computational and Information Systems Laboratory, sponsored by the NSF.

References

Adames, A. F., & Kim, D. (2016). The MJO as a dispersive, convectively coupled moisture wave: Theory and observations. *Journal of the Atmospheric Sciences*, *73*(3), 913–941. https://doi.org/10.1175/JAS-D-15-0170.1

Ahn, M.-S., Kim, D., Sperber, K. R., Kang, I.-S., Maloney, E., Waliser, D., & Hendon, H. (2017). MJO simulation in CMIP5 climate models: MJO skill metrics and process-oriented diagnosis. *Climate Dynamics*, *49*(11), 4023–4045. https://doi.org/10.1007/s00382-017-3558-4

Andersen, J. A., & Kuang, Z. (2012). Moist static energy budget of MJO-like disturbances in the atmosphere of a zonally symmetric aquaplanet. *Journal of Climate*, *25*(8), 2782–2804. https://doi.org/10.1175/jcli-d-11-00168.1

Bui, H. X., & Maloney, E. D. (2018). Changes in Madden-Julian oscillation precipitation and wind variance under global warming. *Geophysical Research Letters*, *45*(14), 7148–7155. https://doi.org/10.1029/2018gl078504

Bui, H. X., & Maloney, E. D. (2020). Changes to the Madden-Julian oscillation in coupled and uncoupled aquaplanet simulations with 4xCO_2. *Journal of Advances in Modeling Earth Systems*, *12*(8), e2020MS002179. https://doi.org/10.1029/2020MS002179

Chang, C.-W. J., Tseng, W.-L., Hsu, H.-H., Keenlyside, N., & Tsuang, B.-J. (2015). The Madden-Julian Oscillation in a warmer world. *Geophysical Research Letters*, *42*(14), 6034–6042. https://doi.org/10.1002/2015gl065095

Das, S., Sengupta, D., & Chakraborty, A. (2019). The Madden-Julian oscillation in an aquaplanet-like general circulation model with and without continents. *Journal of Advances in Modeling Earth Systems*, *11*(5), 1459–1476. https://doi.org/10.1029/2018ms001455

De Deckker, P. (2016). The Indo-Pacific warm pool: Critical to world oceanography and world climate. *Geoscience Letters*, *3*(1), 20. https://doi.org/10.1186/s40562-016-0054-3

Du, D., Subramanian, A. C., Han, W., Chapman, W. E., Weiss, J. B., & Bradley, E. (2024). Increase in MJO predictability under global warming. *Nature Climate Change*, *14*(1), 68–74. https://doi.org/10.1038/s41558-023-01885-0

Fasullo, J., & Webster, P. J. (1999). Warm pool SST variability in relation to the surface energy balance. *Journal of Climate*, *12*(5), 1292–1305. https://doi.org/10.1175/1520-0442(1999)012<1292:wpsvir>2.0.co;2

Fuchs, Ž., & Raymond, D. J. (2017). A simple model of intraseasonal oscillations. *Journal of Advances in Modeling Earth Systems*, *9*(2), 1195–1211. https://doi.org/10.1002/2017MS000963

Hendon, H. H., Wheeler, M. C., & Zhang, C. (2007). Seasonal dependence of the MJO–ENSO relationship. *Journal of Climate*, *20*(3), 531–543. https://doi.org/10.1175/jcli4003.1

Hoskins, B., Neale, R., Rodwell, M., & Yang, G. Y. (1999). Aspects of the large-scale tropical atmospheric circulation. *Tellus*, *51*(1), 33–44. https://doi.org/10.1034/j.1600-0870.1999.t01-1-00004.x

Hoyos, C. D., & Webster, P. J. (2012). Evolution and modulation of tropical heating from the last glacial maximum through the twenty-first century. *Climate Dynamics*, *38*(7), 1501–1519. https://doi.org/10.1007/s00382-011-1181-3

Jiang, X., Adames, Á. F., Kim, D., Maloney, E. D., Lin, H., Kim, H., et al. (2020). Fifty years of research on the Madden-Julian Oscillation: Recent progress, challenges, and perspectives. *Journal of Geophysical Research: Atmospheres*, *125*(17), e2019JD030911. https://doi.org/10.1029/2019JD030911

Kang, I.-S., Liu, F., Ahn, M.-S., Yang, Y.-M., & Wang, B. (2013). The role of SST structure in convectively coupled Kelvin–Rossby waves and its implications for MJO formation. *Journal of Climate*, *26*(16), 5915–5930. https://doi.org/10.1175/jcli-d-12-00303.1

Kim, H. (2024). Decrease in MJO predictability following Indo-Pacific warm pool expansion [Dataset]. *Zenodo*. https://doi.org/10.5281/zenodo.10967437

Kim, H., & Benedict, J. J. (2023). The idealized aquaplanet Maritime Continent barrier effect on the MJO predictability. *Journal of Climate*, *36*(17), 5757–5773. https://doi.org/10.1175/jcli-d-22-0155.1

Kim, H., Vitart, F., & Waliser, D. E. (2018). Prediction of the Madden–Julian oscillation: A review. *Journal of Climate*, *31*(23), 9425–9443. https://doi.org/10.1175/jcli-d-18-0210.1

Klingaman, N. P., & Demott, C. A. (2020). Mean state biases and interannual variability affect perceived sensitivities of the Madden-Julian Oscillation to air-sea coupling. *Journal of Advances in Modeling Earth Systems*, *12*(2), e2019MS001799. https://doi.org/10.1029/2019MS001799

Madden, R., & Julian, P. (1972). Further evidence of global-scale 5-day pressure waves. *Journal of the Atmospheric Sciences*, *29*(8), 1464–1469. https://doi.org/10.1175/1520-0469(1972)029<1464:FEOGSD>2.0.CO;2

Maloney, E. D., Adames, Á. F., & Bui, H. X. (2019). Madden–Julian oscillation changes under anthropogenic warming. *Nature Climate Change*, *9*(1), 26–33. https://doi.org/10.1038/s41558-018-0331-6

Maloney, E. D., & Wolding, B. O. (2015). Initiation of an intraseasonal oscillation in an aquaplanet general circulation model. *Journal of Advances in Modeling Earth Systems*, *7*(4), 1956–1976. https://doi.org/10.1002/2015ms000495

Mariotti, A., Baggett, C., Barnes, E. A., Becker, E., Butler, A., Collins, D. C., et al. (2020). Windows of opportunity for skillful forecasts subseasonal to seasonal and beyond. *Bulletin of the American Meteorological Society*, *101*(5), E608–E625. https://doi.org/10.1175/bams-d-18-0326.1

Medeiros, B. (2020). Aquaplanets as a framework for examination of aerosol effects. *Journal of Advances in Modeling Earth Systems*, *12*(7), e2019MS001874. https://doi.org/10.1029/2019MS001874

Neale, R. B., & Hoskins, B. J. (2000). A standard test for AGCMs including their physical parametrizations: I: The proposal. *Atmospheric Science Letters*, *1*(2), 101–107. https://doi.org/10.1006/asle.2000.0022

Park, I.-H., Yeh, S.-W., Min, S.-K., Ham, Y.-G., & Kirtman, B. P. (2022). Present-day warm pool constrains future tropical precipitation. *Communications Earth & Environment*, *3*(1), 310. https://doi.org/10.1038/s43247-022-00620-5

Pohl, B., & Matthews, A. J. (2007). Observed changes in the lifetime and amplitude of the Madden–Julian oscillation associated with interannual ENSO sea surface temperature anomalies. *Journal of Climate*, *20*(11), 2659–2674. https://doi.org/10.1175/jcli4230.1

Rayner, N. A., Parker, D. E., Horton, E. B., Folland, C. K., Alexander, L. V., Rowell, D. P., et al. (2003). Global analyses of sea surface temperature, sea ice, and night marine air temperature since the late nineteenth century. *Journal of Geophysical Research*, *108*(D14), 4407. https://doi.org/10.1029/2002JD002670

Roxy, M. K., Dasgupta, P., McPhaden, M. J., Suematsu, T., Zhang, C., & Kim, D. (2019). Twofold expansion of the Indo-Pacific warm pool warps the MJO life cycle. *Nature*, *575*(7784), 647–651. https://doi.org/10.1038/s41586-019-1764-4

Rushley, S. S., Kim, D., & Adames, Á. F. (2019). Changes in the MJO under greenhouse gas–induced warming in CMIP5 models. *Journal of Climate*, *32*(3), 803–821. https://doi.org/10.1175/jcli-d-18-0437.1

Shi, X., Kim, D., Adames, Á. F., & Sukhatme, J. (2018). WISHE-moisture mode in an aquaplanet simulation. *Journal of Advances in Modeling Earth Systems*, *10*, 2393–2407. https://doi.org/10.1029/2018MS001441

Sobel, A., & Maloney, E. (2013). Moisture modes and the eastward propagation of the MJO. *Journal of the Atmospheric Sciences*, *70*(1), 187–192. https://doi.org/10.1175/Jas-D-12-0189.1

Subramanian, A., Jochum, M., Miller, A. J., Neale, R., Seo, H., Waliser, D., & Murtugudde, R. (2014). The MJO and global warming: A study in CCSM4. *Climate Dynamics*, *42*(7), 2019–2031. https://doi.org/10.1007/s00382-013-1846-1

Suematsu, T., & Miura, H. (2018). Zonal SST difference as a potential environmental factor supporting the longevity of the Madden–Julian oscillation. *Journal of Climate*, *31*(18), 7549–7564. https://doi.org/10.1175/jcli-d-17-0822.1

Suematsu, T., & Miura, H. (2022). Changes in the eastward movement speed of the Madden–Julian oscillation with fluctuation in the Walker circulation. *Journal of Climate*, *35*(1), 211–225. https://doi.org/10.1175/jcli-d-21-0269.1

Suematsu, T., Miura, H., Kodama, C., & Takasuka, D. (2022). Deceleration of Madden–Julian oscillation speed in NICAM AMIP-type simulation associated with biases in the Walker circulation strength. *Geophysical Research Letters*, *49*(11), e2022GL098628. https://doi.org/10.1029/2022GL098628

Wang, B., & Rui, H. (1990). Dynamics of the coupled moist Kelvin–Rossby wave on an equatorial β-plane. *Journal of the Atmospheric Sciences*, *47*(4), 397–413. https://doi.org/10.1175/1520-0469(1990)047<0397:dotcmk>2.0.co;2

Wang, B., & Wang, T. (2023). How the 1999 climate shift has changed MJO propagation diversity. *Journal of Climate*, *36*(10), 3523–3535. https://doi.org/10.1175/jcli-d-22-0749.1

Weller, E., Min, S.-K., Cai, W., Zwiers, F. W., Kim, Y.-H., & Lee, D. (2016). Human-caused Indo-Pacific warm pool expansion. *Science Advances*, *2*(7), e1501719. https://doi.org/10.1126/sciadv.1501719

Wheeler, M., & Kiladis, G. N. (1999). Convectively coupled equatorial waves: Analysis of clouds and temperature in the wavenumber–frequency domain. *Journal of the Atmospheric Sciences*, *56*(3), 374–399. https://doi.org/10.1175/1520-0469(1999)056<0374:ccewao>2.0.co;2

Wheeler, M. C., & Hendon, H. H. (2004). An all-season real-time multivariate MJO index: Development of an index for monitoring and prediction. *Monthly Weather Review*, *132*(8), 1917–1932. https://doi.org/10.1175/1520-0493(2004)132<1917:aarmmi>2.0.co;2

Woolnough, S. J., Slingo, J. M., & Hoskins, B. J. (2000). The relationship between convection and sea surface temperature on intraseasonal timescales. *Journal of Climate*, *13*(12), 2086–2104. https://doi.org/10.1175/1520-0442(2000)013<2086:trbcas>2.0.co;2

Wu, X., Reed, K. A., Wolfe, C. L. P., Marques, G. M., Bachman, S. D., & Bryan, F. O. (2021). The dependence of tropical modes of variability on zonal asymmetry. *Geophysical Research Letters*, *48*(17), e2021GL093966. https://doi.org/10.1029/2021GL093966

19448007, 2024, 13, Downloaded from https://agupubs.onlinelibrary.wiley.com/doi/10.1029/2024GL108849 by Ewha Womans University Library, Wiley Online Library on [30/10/2024]. See the Terms and Conditions (https://onlinelibrary.wiley.com/terms-and-conditions) on Wiley Online Library for rules of use; OA articles are governed by the applicable Creative Commons License